

UC Berkeley

UC Berkeley Previously Published Works

Title

Operation of Flying Capacitor Multilevel Converters At and Above Resonance

Permalink

<https://escholarship.org/uc/item/9bx6q4pt>

ISBN

9781665410816

Authors

Brooks, Nathan C
Coday, Samantha
Blackwell, Margaret E
[et al.](#)

Publication Date

2022-06-23

DOI

10.1109/compel53829.2022.9830004

Copyright Information

This work is made available under the terms of a Creative Commons Attribution License, available at <https://creativecommons.org/licenses/by/4.0/>

Peer reviewed

© 2022 IEEE

2022 IEEE 23rd Workshop on Control and Modeling for Power Electronics (COMPEL), Tel Aviv, Israel,
June 2022

Operation of Flying Capacitor Multilevel Converters At and Above Resonance

N. C. Brooks
S. Coday
M. E. Blackwell
R. A. Abramson
N. M. Ellis
R. C. N. Pilawa-Podgurski

Personal use of this material is permitted. Permission from IEEE must be obtained for all other uses, in any current or future media, including reprinting/republishing this material for advertising or promotional purposes, creating new collective works, for resale or redistribution to servers or lists, or reuse of any copyrighted component of this work in other works.

Operation of Flying Capacitor Multilevel Converters At and Above Resonance

Nathan C. Brooks, Samantha Coday, Margaret E. Blackwell,

Rose A. Abramson, Nathan M. Ellis, and Robert C. N. Pilawa-Podgurski

Department of Electrical Engineering and Computer Sciences, University of California, Berkeley

Email: {nathanbrooks, scoday, blackwell, rose_abramson, nathanmilesellis, pilawa}@berkeley.edu

Abstract—The flying capacitor multilevel (FCML) converter has shown promise for high step-up/down conversion ratio applications due to its relatively low switch stress and small inductor volume. For higher level-count ($N \geq 3$) variations of this topology, there is limited research on resonant mode operation, despite its potential to yield considerable performance benefits for fixed conversion ratio applications. When operating resonantly, the decreased inductance requirement compared to regulated operation can further reduce the magnetic volume and improve transient response, while also allowing for zero-voltage/zero-current switching (ZCS/ZVS). This work presents and analyzes a clocking scheme required to operate an $N:1$ FCML converter both at-resonance and above-resonance, while maintaining minimum current ripple for reduced losses. A complete derivation is presented, enabling the calculation of precise phase durations as a function of switching frequency. Moreover, a 5:1 FCML hardware prototype is demonstrated, verifying intended operation both at- and above-resonance, in addition to highlighting the achievable loss reduction with the proposed switching scheme.

I. INTRODUCTION

The flying capacitor multilevel (FCML) converter [1] has gained popularity due to its high power density and high efficiency for both step-up [2] and step-down conversion [3], over a very wide conversion range [4]–[6]. This topology is often discussed as an attractive alternative to conventional buck-type or boost-type topologies due to its ability to regulate the output, its greatly reduced inductance requirements; and its decreased switch stress on the active devices, which allows the designer to take advantage of better figures-of-merit lower voltage switches [7], [8]. However, the FCML converter can also be operated in a resonant mode as a fixed-ratio converter similar to other hybrid resonant switched-capacitor (SC) converters [9], [10]. As discussed in [11], [12], resonant operation of hybrid SC converters eliminates capacitor charge sharing losses, and allows for zero-current/voltage switching (ZCS/ZVS) to decrease switching losses. Furthermore, previous work has shown that operating hybrid SC converters above-resonance—at the fast-switching limit (FSL) [13]—can reduce the output impedance [14] and decrease sensitivity to component variation [15]. While operating above-resonance precludes ZCS, conduction and ac losses can be reduced due to the decreased rms currents compared to at-resonance operation. For high current applications, this is often a desirable trade-off.

Unlike many other hybrid SC converters, higher order ($N \geq 3$) resonant FCML converters require multi-resonant

operation, with non-uniform resonant phase durations dependent on the level count, flying capacitance, and inductance. Previous work in [9], [14] proposed timings for a general 2:1 resonant converter, as all hybrid SC converters collapse to this equivalent circuit for $N = 2$; however, this analysis was not extended to higher level converters. Furthermore, [10] explored above-resonance operation of $N = 3$ and $N = 6$ FCML converters, but used a valley current control scheme to converge on optimal phase durations through active feedback. As such, no closed-form analytical solution to ideal phase timings has been published.

This work expands on prior analysis and provides an analytical solution to the optimal phase durations for a generic FCML converter operating at a fixed $N:1$ conversion for both at-resonance and above-resonance operation. The analysis presented here also provides a more general framework for analyzing other at- and above-resonance hybrid switched capacitor converters, though the FCML converter represents a more complex case due to the dependence of the phase durations on the relationship between the converter switching frequency and its natural resonant frequencies. Lastly, experimental results for a 5:1 FCML converter are presented, validating the proposed analysis and demonstrating FCML performance at and above resonance.

II. THEORY OF OPERATION

Fig. 1a shows a generic step-down $N:1$ FCML converter, where the input and output voltages are denoted as V_{HI} and V_{LO} , respectively. In this work, the parameter N refers to both the conversion ratio of the FCML converter as well as the number of complementary switch-pairs, $S_{NA/B}$. While the FCML converter can operate in resonance mode with fixed conversion ratios equal to or greater than $1/N$ (i.e., $N:2$, $N:3$, ...), this work will analyze the most extreme conversion ratio, $N:1$.

The gate timings of each switch pair, as shown in Fig. 2, are adjusted to ensure a half-sine-wave (at resonance) or a symmetric sine-wave segment (above resonance) inductor current in each phase, as illustrated in Fig. 3. To determine appropriate phase durations, charge flow analysis is performed [13]. While this analysis is suitable for any $N:1$ FCML converter, Fig. 1 depicts the circuit schematics for each phase of an example 5:1 step-down FCML converter. Here, the charge q_H is defined as the product of the average current supplied by the high-side voltage, V_{HI} , and the switching period: $q_H = I_{HI} \cdot T_{sw}$.

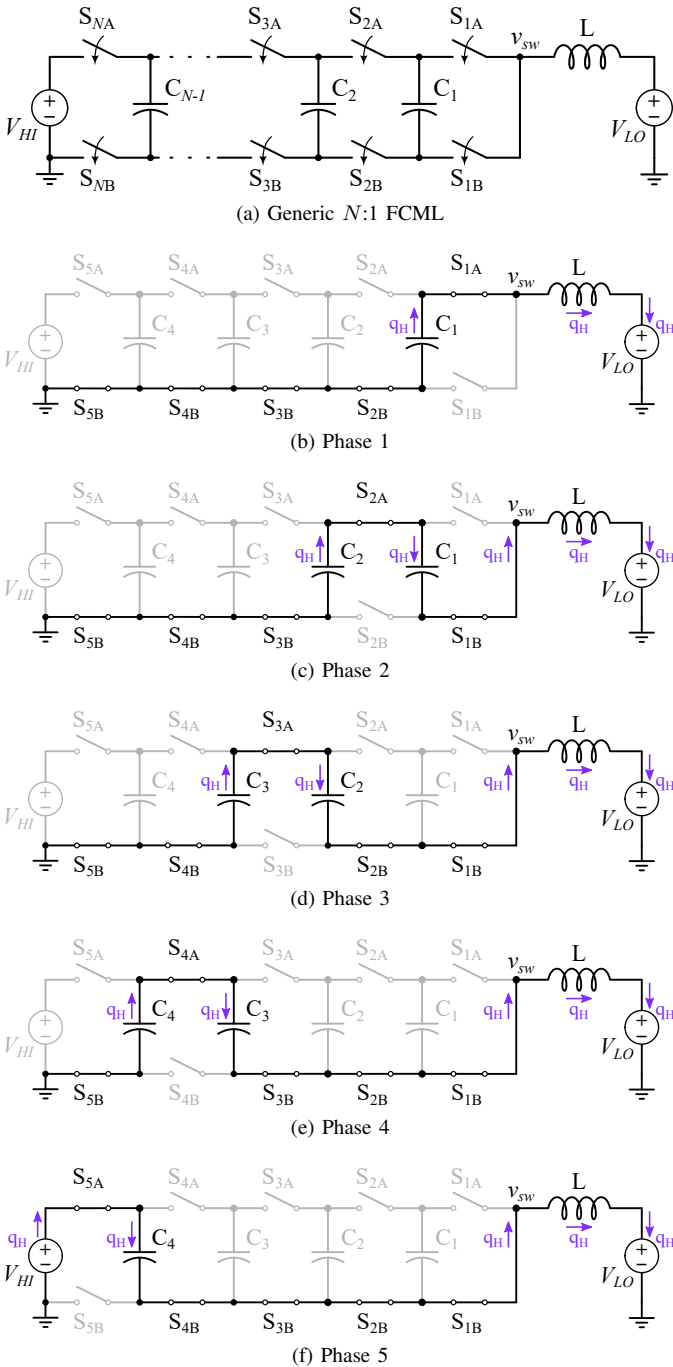


Fig. 1: Schematic for (a) a generic $N:1$ FCML converter, and (b)-(f) a 5:1 FCML converter, highlighting the charge flow during each phase, normalized with respect to high-side input charge quantity q_H .

Phase 5 (Fig. 1f) is the only phase in which V_{HI} is connected, therefore, the charge supplied by V_{HI} in this phase must equal q_H .

Following the charge flow across phases, each flying capacitor is charged by q_H in one phase and discharged by q_H in one other phase, thereby maintaining charge balance across the capacitors in periodic steady-state. Because each flying

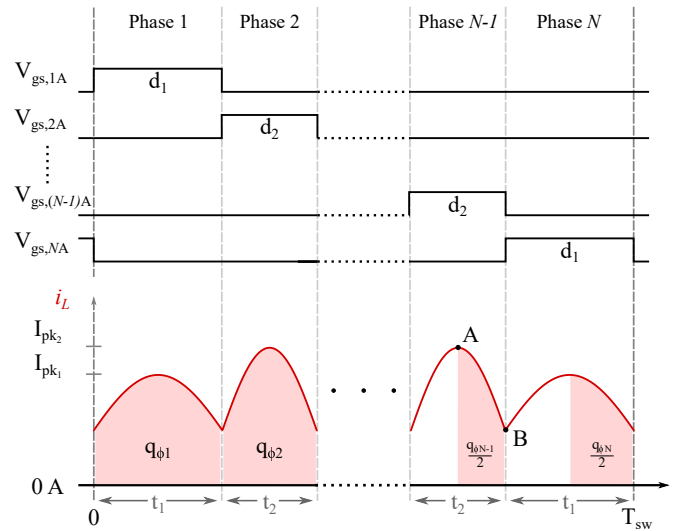


Fig. 2: Modulation scheme at- and above-resonance for $N:1$ FCML. The current i_L is shown for above-resonance operation.

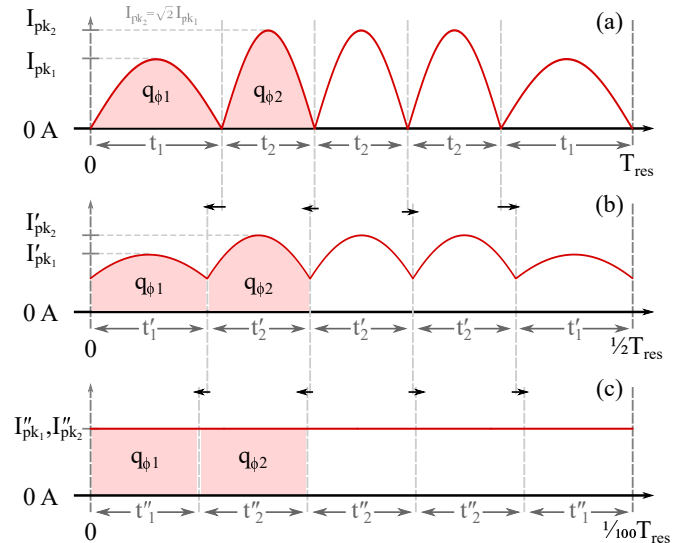


Fig. 3: Example 5:1 FCML inductor current waveforms at (a) $\Gamma = 1$, (b) $\Gamma = 2$, and (c) $\Gamma = 100$.

capacitor is charged/discharged by the same charge quantity, equating all capacitances C_1 through C_{N-1} to an equivalent value, C_0 , enforces equivalent voltage ripple magnitude on each of the flying capacitors. Finally, one q_H quantity is delivered to the low-side voltage, V_{LO} , through inductor L during *each* of the five phases (N phases). Thus, the net charge delivered to V_{LO} over N phases is $N \cdot q_H$, affirming the conversion ratio.

III. CALCULATING PHASE DURATIONS

To calculate ideal timing durations of each phase in periodic steady-state, the inductor current is assumed to start and end each phase at the same value, implying zero net volt-seconds across the inductor within each phase and minimized rms current ripple within a total period for reduced conduction

and ac losses. Furthermore, for this analysis a high Q-factor is reasonably assumed for each phase configuration, leading to sinusoidal behavior with negligible damping.

A. At Resonance ($\Gamma = 1$)

As shown in Fig. 1b and Fig. 1f, only one flying capacitor with capacitance C_0 is connected in series with the inductor during phase 1 and phase N , allowing their resonant frequency, ω_{r1} , to be calculated as

$$\omega_{r1} = \frac{1}{\sqrt{LC_0}}. \quad (1)$$

Similarly, all other phases (2, 3, ..., $N-1$) are topologically equivalent, as they have two series-connected flying capacitors connected with the inductor. The resonant frequency in these phases can therefore be calculated as

$$\omega_{r2} = \frac{1}{\sqrt{L \cdot (\frac{1}{2}C_0)}}. \quad (2)$$

The relationship between the two resonant frequencies is then

$$\sqrt{2} \omega_{r1} = \omega_{r2}. \quad (3)$$

Since equal charge q_H flows through the inductor during each phase ($q_H = I_{L,avg_i} \cdot t_{\phi_i}$), the relationship between the peak inductor currents, I_{pk1} and I_{pk2} , during each phase is determined by their resonant frequency ratio, yielding $\sqrt{2} I_{pk1} = I_{pk2}$. Exact expressions relating these peak currents to the output current I_{out} can be derived by calculating the rms value of the inductor current, as given below:

$$\frac{I_{pk2}}{I_{out}} = \frac{\pi}{2} \left(\frac{2\sqrt{2} + N - 2}{N} \right) \quad (4)$$

$$\frac{I_{pk1}}{I_{out}} = \frac{\pi}{2} \left(\frac{2\sqrt{2} + N - 2}{\sqrt{2}N} \right) \quad (5)$$

Example inductor current waveforms while operating at-resonance can be seen in Fig. 3a. Note at resonance, the inductor current hits zero at each phase transition, thereby achieving full ZCS.

B. Above Resonance ($\Gamma > 1$)

In considering operation of the FCML converter above-resonance, we define the parameter Γ in (6), which relates the actual switching frequency of a full period f_{sw} to its inherent natural resonant value (dependent only on the inductance and capacitance values), $f_{sw,res}$.

$$\Gamma = \frac{f_{sw}}{f_{sw,res}} = \frac{T_{sw,res}}{T_{sw}} \quad (6)$$

In the at-resonant case, Γ is unity. In above-resonant operation, the switching frequency and Γ both increase.

Fig 3b shows the inductor current waveform at a switching frequency twice the resonant frequency, i.e., $\Gamma = 2$. As the switching frequency is now higher than the natural resonant frequency of the circuit, the inductor current does not complete a full resonant half-cycle within each phase. Instead, the

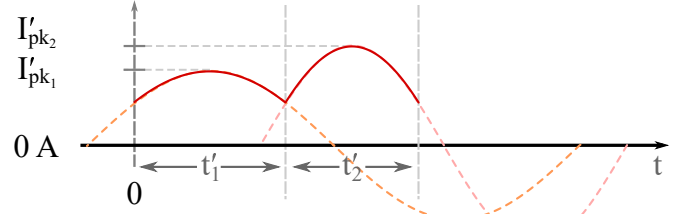


Fig. 4: Partial sine wave extension for inductor current i_L operating above resonance.

inductor current follows a segment of the rectified sinusoid, symmetric about its peak value. While the overall inductor current now has a dc offset, the inductor waveform within each phase is still defined by a zero-centered sinusoid, as shown in Fig. 4. This partial sinusoidal waveform operates at the natural resonant frequency of the equivalent circuit during that phase. Since the inductor current no longer reaches zero at the phase transitions, the converter has lost the ability to achieve ZCS. However, the peak-to-peak ripple of the inductor current has been greatly reduced, allowing for much lower conduction losses.

Fig. 3c shows the FCML inductor current waveforms for a switching frequency significantly greater than resonance: $\Gamma = 100$. For this operating condition, both the phase durations and peak inductor currents are effectively equal across all phases, and the inductor current appears as a constant dc waveform. As $\Gamma \rightarrow \infty$, the current ripple decreases towards zero, resulting in a dc current waveform. The same charge is delivered to the output in each phase, therefore the time spent in each phase must be the same.

To derive the proper time duration of each phase for different Γ and N , a ‘charge balance’ and ‘continuous current’ constraint between phases is imposed on the inductor current.

1) ‘Charge balance’ constraint: The charge transferred, q_{ϕ_i} , during a phase ϕ_i is computed by integrating the instantaneous inductor current waveform $i_L(t)$ —which is known generally for a resonant LC circuit—over the duration of each phase. Quarter-wave symmetry of the sinusoidal $i_L(t)$ (see points A to B in Fig. 2) is utilized to simplify the integrations for each phase by evaluating a cosine integral centered on the peak of the inductor current.

$$q_{\phi_1} = \int_{-\frac{t_1}{2}}^{\frac{t_1}{2}} I_{pk1} \cos(\omega_{r1}t) dt = \frac{2I_{pk1}}{\omega_{r1}} \sin\left(\omega_{r1} \frac{t_1}{2}\right) \quad (7)$$

$$q_{\phi_2} = \int_{-\frac{t_2}{2}}^{\frac{t_2}{2}} I_{pk2} \cos(\omega_{r2}t) dt = \frac{2I_{pk2}}{\omega_{r2}} \sin\left(\omega_{r2} \frac{t_2}{2}\right) \quad (8)$$

The per-phase charges (7) and (8) are substituted into the FCML charge-balance relation (i.e., $q_{\phi_1} = q_{\phi_2} = \dots = q_{\phi_N}$) to derive the first constraining equation:

$$q_{\phi_1} = q_{\phi_2} \Rightarrow \frac{I_{pk1}}{I_{pk2}} = \frac{\omega_{r1}}{\omega_{r2}} \cdot \frac{\sin\left(\frac{1}{2}\omega_{r2}t_2\right)}{\sin\left(\frac{1}{2}\omega_{r1}t_1\right)} \quad (9)$$

2) ‘Continuous current’ constraint: The second constraint imposes a continuous inductor current waveform, $i_L(t)$, be-

tween phases, as in (10). Moreover, the instantaneous current is assumed equal at all phase transitions (net-zero volt-seconds across the inductor).

This requirement—enforcing equivalent valley currents—yields an inductor current with minimized peak, peak-to-peak, and rms values, thereby minimizing inductor saturation limits, conduction losses, and switch voltage ratings.

$$\begin{aligned} I_{pk_1} \cos\left(\omega_{r1} \frac{t_1}{2}\right) &= I_{pk_2} \cos\left(\omega_{r2} \frac{t_2}{2}\right) \\ \Rightarrow \frac{I_{pk_1}}{I_{pk_2}} &= \frac{\cos\left(\frac{1}{2}\omega_{r2}t_2\right)}{\cos\left(\frac{1}{2}\omega_{r1}t_1\right)} \end{aligned} \quad (10)$$

3) *Solving for phase durations:* Substituting the ‘charge balance’ constraint (9) into the ‘continuous current’ constraint (10) yields an implicit equation (11) of t_1 and t_2 , where the per-phase resonant frequencies ω_{r1} and ω_{r2} are known quantities for a specified L and C_0 .

$$\frac{\omega_{r1}}{\omega_{r2}} \cdot \frac{\sin\left(\frac{1}{2}\omega_{r2}t_2\right)}{\sin\left(\frac{1}{2}\omega_{r1}t_1\right)} = \frac{\cos\left(\frac{1}{2}\omega_{r2}t_2\right)}{\cos\left(\frac{1}{2}\omega_{r1}t_1\right)} \quad (11)$$

A third constraining equation relates the sum of all phase durations to the switching period T_{sw} by

$$T_{sw} = \sum_{i=1}^N t_{\phi_i} = 2t_1 + (N-2)t_2. \quad (12)$$

Since $\sqrt{2}\omega_{r1} = \omega_{r2}$ (3) for the resonant FCML converter, the implicit equation in (11) reduces no further and thus the phase durations cannot be determined analytically. Equation (11) can be rearranged to construct a minimization function $f(t_1, t_2)$ in (13), using (12) as a constraint. Using trigonometric identities, one can rearrange the expression in (11) to numerically solve for t_1 (and t_2).

$$\begin{aligned} f(t_1, t_2) = 0 &= \left| \sin\left(\frac{1}{2}\omega_{r1}t_1 - \frac{1}{2}\omega_{r2}t_2\right) \right. \\ &\quad \left. - \frac{\omega_{r1} - \omega_{r2}}{\omega_{r1} + \omega_{r2}} \cdot \sin\left(\frac{1}{2}\omega_{r1}t_1 + \frac{1}{2}\omega_{r2}t_2\right) \right| \end{aligned} \quad (13)$$

From inspection of the numerical solution, an accurate closed-form expression of the relative phase durations t_1/T_{sw} and t_2/T_{sw} can be approximated in (14) and (15) as a function of N and Γ only.

$$\begin{aligned} \frac{t_1}{T_{sw}} &\approx \left(\frac{1}{N} - \frac{\sqrt{2}}{2\sqrt{2} + N - 2} \right) \cdot \frac{\Gamma}{\pi} \sin\left(\frac{\pi}{\Gamma}\right) \\ &\quad + \frac{\sqrt{2}}{2\sqrt{2} + N - 2} \end{aligned} \quad (14)$$

$$\begin{aligned} \frac{t_2}{T_{sw}} &\approx \left(\frac{1}{N} - \frac{1}{2\sqrt{2} + N - 2} \right) \cdot \frac{\Gamma}{\pi} \sin\left(\frac{\pi}{\Gamma}\right) \\ &\quad + \frac{1}{2\sqrt{2} + N - 2} \end{aligned} \quad (15)$$

Fig. 5 shows both the numerical and analytical approxima-

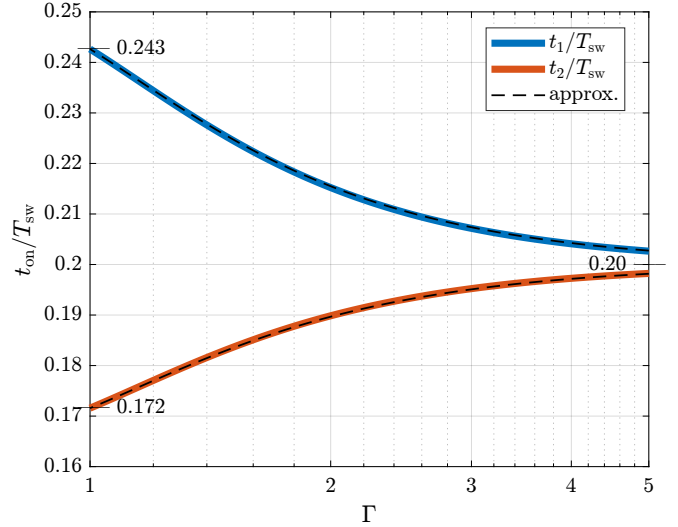


Fig. 5: Numerical solution of relative phase durations t_1/T_{sw} and t_2/T_{sw} for a 5:1 FCML across Γ . The closed-form approximations are superimposed with dashed lines.

tions for the t_1 and t_2 time durations for an $N = 5$ FCML example. The error between the numerical and analytical results are negligible, validating the accuracy of (14) and (15).

C. Inductor Current

The phase duration expressions in (14) and (15) can be used to derive an approximation for the peak inductor current to output current ratio $I_{L,pk}/I_{out}$ by manipulating charge relationships in (7) and (8). Peak inductor current occurs during phases 2 through $N - 1$ (for $N > 2$), while two flying capacitors are connected in series:

$$\frac{I_{L,pk}}{I_{out}} \approx \begin{cases} \frac{I_{pk_2}}{I_{out}}, & N \geq 3 \\ \frac{I_{pk_1}}{I_{out}}, & N = 2 \end{cases} \quad (16)$$

where the individual ratios in each phase are derived as

$$\frac{I_{pk_2}}{I_{out}} \approx \frac{\left(\frac{\pi(2\sqrt{2} + N - 2)}{2N\Gamma} \right)}{\sin\left(\frac{\sqrt{2} - 1}{N} \sin\left(\frac{\pi}{\Gamma}\right) + \frac{\pi}{2\Gamma} \right)} \quad (17)$$

$$\frac{I_{pk_1}}{I_{out}} \approx \frac{\left(\frac{\pi(2\sqrt{2} + N - 2)}{2\sqrt{2}N\Gamma} \right)}{\sin\left((\sqrt{2} - 2) \frac{N - 2}{4N} \sin\left(\frac{\pi}{\Gamma}\right) + \frac{\pi}{2\Gamma} \right)} \quad (18)$$

Fig. 6 illustrates for increasing Γ and increasing N , the peak inductor current ratio $I_{L,pk}/I_{out}$ decreases monotonically. Consequently, conduction losses in the flying capacitors and inductor are also expected to decrease. When at resonance (i.e., $\Gamma = 1$), (17) and (18) reduce to the exact expressions in (4)

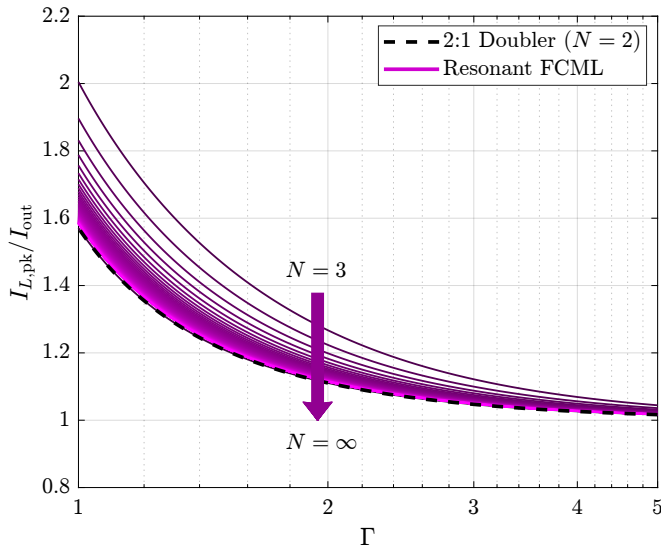


Fig. 6: Γ versus the inductor peak current to output current ratio for all N .

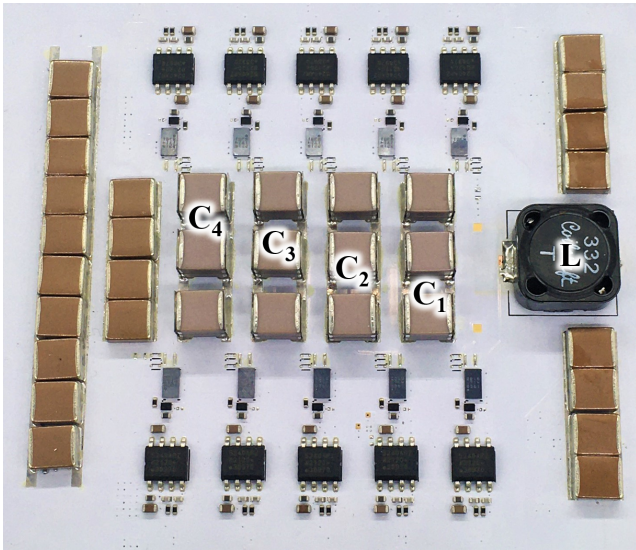


Fig. 7: Annotated photograph of the constructed 5:1 FCML hardware prototype.

and (5), respectively, further validating the model's accuracy above resonance.

IV. EXPERIMENTAL VALIDATION

A 5:1 FCML converter was built, as shown in Fig. 7, to verify the proposed phase durations at and above resonance. The relevant components selected for this prototype are shown in Table I. Class I multilayer ceramic capacitors were chosen as they have stable capacitance over temperature and voltage bias and are thus suitable for operation at an exact resonance point. Furthermore, Class I capacitors are better for validating the accuracy of the proposed timing calculation method, as the effect of non-idealities and capacitance variation can be neglected. However, the time duration calculation method does hold for nonlinear capacitances—the resonant frequencies dur-

TABLE I: Component Details

Component	Description	Part Name
S_{1-5A}, S_{1-5B}	100 V, 3.2 m Ω GaN-FET	EPC2218
C_{1-4}	$3 \times 0.3 \mu\text{F}$, C0G, 250V	CKG57NC0G2E304J500JH
L	3.39 μH	MSS1260-332NLD
R_{GATE}	37.5 Ω , 0402	CR0402-16W-35R7FT
Gate Driver	5 V, 7 A/5 A	LMG1020
Isolator	Power and Signal	ADUM5240

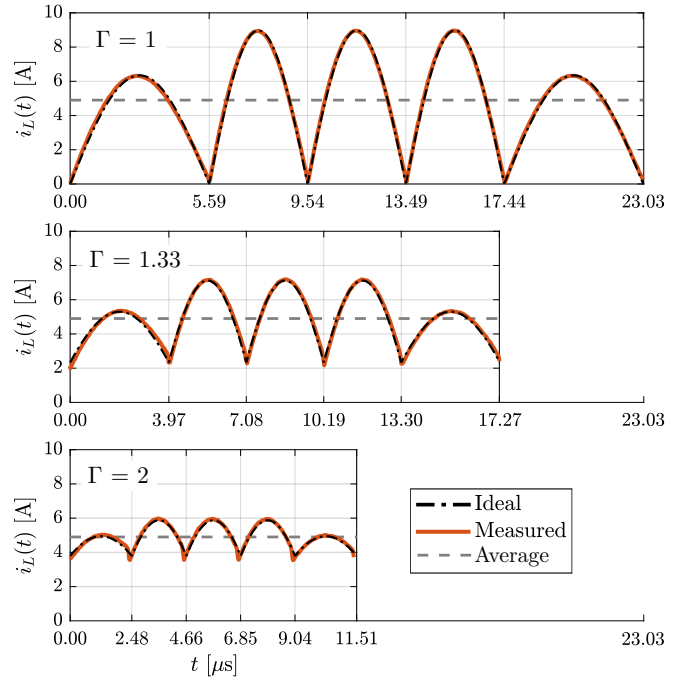


Fig. 8: Measured versus ideal inductor current waveforms for various Γ ($N = 5$, $I_{out} = 4.9$ A). As Γ increases, all phase durations approach equivalency.

ing each phase may also then be dependent on bias voltage and operating temperature. Moreover, the chosen inductor is constructed using a shielded ferrite core. Ferrite was chosen as it is reasonably stable over frequency and dc-bias current, further simplifying the validation of the proposed control scheme. With the selected flying capacitance and inductance, the switching frequency of the converter at resonance (i.e., $\Gamma = 1$) is $f_{sw,res} = 43.4$ kHz.

A. Comparison of Derived Phase Durations

Testing of the prototype validated that the approximate phase durations derived in (14) and (15) match experimental results both at and above resonance (i.e., $\Gamma \geq 1$) as shown in Fig. 8. Fig. 9 presents the measured inductor current comparing operation with the derived time durations as given in (14) and (15), compared to an incorrect timing scheme using all equal phase durations. At $\Gamma = 1.25$, the measured efficiency η in Fig. 10 illustrates up to a 15% decrease in converter losses across the load range. Specifically at a load

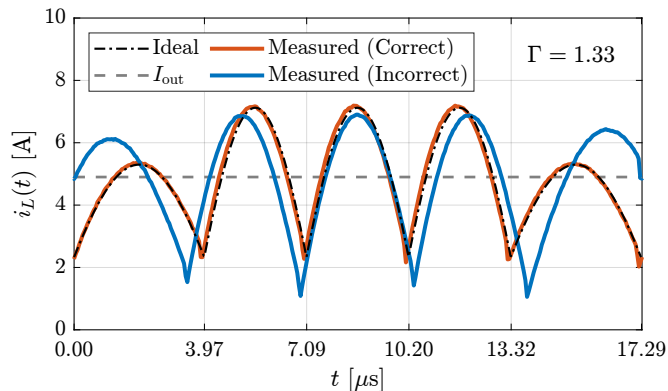


Fig. 9: Measured versus ideal inductor current waveforms with the calculated phase durations (correct) versus all equivalent durations (incorrect) at $\Gamma = 1.33$ ($I_{out} = 4.9$ A).

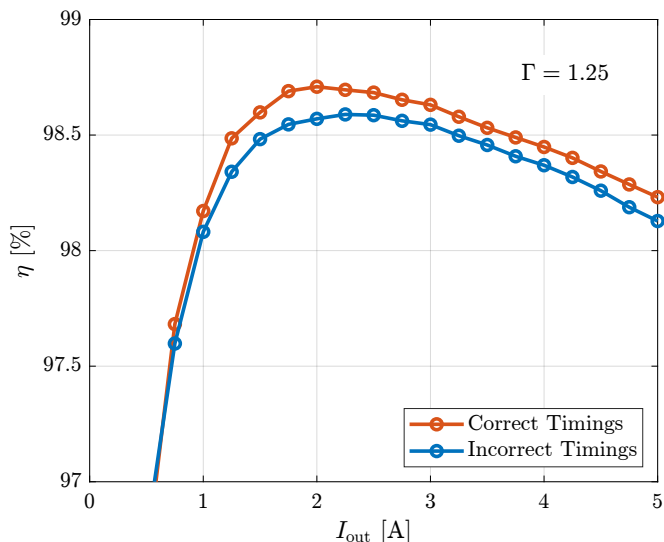


Fig. 10: Comparison of measured efficiency for operation with the calculated phase durations (correct), versus all equivalent durations (incorrect).

of $I_{out} = 4.9$ A, the rms of the correctly and incorrectly timed inductor current waveforms are 5.08 A and 5.17 A, respectively, which although slight, noticeably impacts the conduction losses.

B. Efficiency Analysis

Efficiency, η , was also measured across a range of output current I_{out} and Γ . Fig. 11 illustrates an interpolated contour of these measured efficiencies. It also denotes the maximum output current of the converter is bounded by the inductor saturation current limit which can be exceeded either by increasing the output current or by increasing the peak-to-peak ripple (i.e. decreasing Γ). For example, this converter prototype cannot achieve $\Gamma < 2$ for $I_{out} > 10$ A as the peak inductor current under such high ripple would exceed the saturation limit.

As Γ increases above unity (i.e., f_{sw} increases), the efficiency is maximized in the region $1.1 < \Gamma < 1.4$. Note effi-

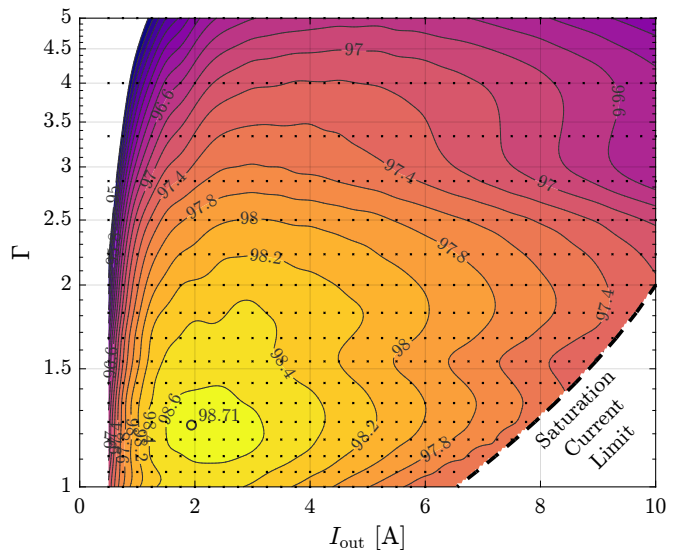


Fig. 11: Measured efficiency, η , interpolation contour with swept I_{out} and Γ . Measured datapoints are denoted. $N = 5$, $V_{HI} = 200$ V, $L = 3.39$ μ H, $C_0 = 0.93$ μ F ($f_{sw,res} = 43.4$ kHz).

ciency does not monotonically increase with increasing Γ as the reduction in conduction losses are offset by an increase in switching losses. The optimal operating point occurs where the switching losses and conduction losses are balanced. As shown in Fig. 11, peak efficiency is achieved when the converter is operated slightly above resonance, where the reduction in current ripple has the most profound effect on the conduction losses. Above this operating condition, the reduced ripple gives diminishing returns in terms of decreasing conduction losses, and the converter's efficiency suffers more from the increased switching losses.

The hardware prototype demonstrates the benefits of above-resonance operation ($\Gamma > 1$), in terms of improved overall efficiency, even at the expense of losing ZCS—a conclusion shared by [14], [15].

V. CONCLUSION

This work derives the closed-form solution for the phase durations required to operate an $N:1$ FCML at and above resonance, while simultaneously minimizing rms inductor current ripple for reduced overall converter loss. Furthermore, a general method for analyzing above-resonance behavior of hybrid switched-capacitor converters has been presented. The hardware prototype results for the 5:1 FCML converter match simulation closely and validate the presented operation scheme.

ACKNOWLEDGMENT

The authors gratefully acknowledge support for this work in part from the National Science Foundation (NSF), as well as the U.S. Department of Defense (DoD). Margaret Blackwell was supported by the NSF Graduate Research Fellowship Program under Grant No. DGE-1752814. Rose Abramson was supported by the U.S. DoD through the National Defense Science & Engineering Graduate (NDSEG) Fellowship Program.

REFERENCES

- [1] T. A. Meynard and H. Foch, "Multi-level conversion: high voltage choppers and voltage-source inverters," in *Power Electronics Specialists Conference, 1992. PESC '92 Record., 23rd Annual IEEE*, Jun 1992, pp. 397–403 vol.1.
- [2] Z. Liao, Y. Lei, and R. C. N. Pilawa-Podgurski, "Analysis and design of a high power density flying-capacitor multilevel boost converter for high step-up conversion," *IEEE Transactions on Power Electronics*, vol. 34, no. 5, pp. 4087–4099, 2019.
- [3] D. Chou, Y. Lei, and R. C. N. Pilawa-Podgurski, "A zero-voltage-switching, physically flexible multilevel gan dc-dc converter," *IEEE Transactions on Power Electronics*, vol. 35, no. 1, pp. 1064–1073, 2020.
- [4] T. Modeer, N. Pallo, T. Foulkes, C. B. Barth, and R. C. N. Pilawa-Podgurski, "Design of a GaN-based interleaved nine-level flying capacitor multilevel inverter for electric aircraft applications," *IEEE Transactions on Power Electronics*, vol. 35, no. 11, pp. 12 153–12 165, 2020.
- [5] E. Candan, N. C. Brooks, A. Stillwell, R. A. Abramson, J. Strydom, and R. C. N. Pilawa-Podgurski, "A six-level flying capacitor multilevel converter for single-phase buck-type power factor correction," *IEEE Transactions on Power Electronics*, vol. 37, no. 6, pp. 6335–6348, 2022.
- [6] J. Azurza Anderson, G. Zulauf, P. Papamanolis, S. Hobi, S. Mirić, and J. W. Kolar, "Three levels are not enough: Scaling laws for multilevel converters in ac/dc applications," *IEEE Transactions on Power Electronics*, vol. 36, no. 4, pp. 3967–3986, 2021.
- [7] J. T. Stauth, "Pathways to mm-scale dc-dc converters: Trends, opportunities, and limitations," in *2018 IEEE Custom Integrated Circuits Conference (CICC)*, 2018, pp. 1–8.
- [8] J. Azurza Anderson, G. Zulauf, J. W. Kolar, and G. Deboy, "New figure-of-merit combining semiconductor and multi-level converter properties," *IEEE Open Journal of Power Electronics*, vol. 1, pp. 322–338, 2020.
- [9] K. Kesarwani and J. T. Stauth, "Resonant and multi-mode operation of flying capacitor multi-level dc-dc converters," in *2015 IEEE 16th Workshop on Control and Modeling for Power Electronics (COMPEL)*, 2015, pp. 1–8.
- [10] C. Schaefer, J. Rentmeister, and J. T. Stauth, "Multimode operation of resonant and hybrid switched-capacitor topologies," *IEEE Transactions on Power Electronics*, vol. 33, no. 12, pp. 10 512–10 523, Dec 2018.
- [11] Y. Lei and R. C. N. Pilawa-Podgurski, "A general method for analyzing resonant and soft-charging operation of switched-capacitor converters," *IEEE Transactions on Power Electronics*, vol. 30, no. 10, pp. 5650–5664, 2015.
- [12] S. R. Pasternak, M. H. Kiani, J. S. Rentmeister, and J. T. Stauth, "Modeling and performance limits of switched-capacitor dc-dc converters capable of resonant operation with a single inductor," *IEEE Journal of Emerging and Selected Topics in Power Electronics*, vol. 5, no. 4, pp. 1746–1760, 2017.
- [13] M. Seeman and S. Sanders, "Analysis and optimization of switched-capacitor dc-dc converters," *Power Electronics, IEEE Transactions on*, vol. 23, no. 2, pp. 841–851, March 2008.
- [14] J. S. Rentmeister and J. T. Stauth, "Multi-mode operation of resonant switched capacitor converters for optimized efficiency," in *2018 IEEE 19th Workshop on Control and Modeling for Power Electronics (COMPEL)*, 2018, pp. 1–7.
- [15] Z. Ye, Y. Lei, and R. C. N. Pilawa-Podgurski, "The cascaded resonant converter: A hybrid switched-capacitor topology with high power density and efficiency," *IEEE Transactions on Power Electronics*, vol. 35, no. 5, pp. 4946–4958, 2020.